

Toward An Objective Enhanced-V Detection Algorithm

Jason C. Brunner, Wayne F. Feltz, Steven A. Ackerman

Cooperative Institute for Meteorological Satellite Studies (CIMSS), University of Wisconsin-Madison
Madison, Wisconsin, U.S.A.

John F. Moses

NASA Goddard Space Flight Center
Washington D.C., U.S.A.

Robert M. Rabin

NOAA/National Severe Storms Laboratory
Norman, Oklahoma, U.S.A.

ABSTRACT

The area of coldest cloud tops above thunderstorms sometimes has a distinct V or U shape. This pattern, often referred to as an “enhanced-V” signature, has been observed to occur during and preceding severe weather. This study describes an algorithmic approach to objectively detect overshooting tops, temperature couplets, and enhanced-V features with observations from the Geostationary Operational Environmental Satellite and Low Earth Orbit data. The methodology consists of temperature, temperature difference, and distance thresholds for the overshooting top and temperature couplet detection parts of the algorithm and consists of cross correlation statistics of pixels for the enhanced-V detection part of the algorithm. The effectiveness of the overshooting top and temperature couplet detection components of the algorithm is examined using GOES and MODIS image data for case studies in the 2003-2006 seasons. The main goal is for the algorithm to be useful for operations with future sensors, such as GOES-R.

1. INTRODUCTION

Many studies have observed and analyzed the enhanced-V feature (McCann 1983; Negri 1982; Heymsfield et al. 1983a, 1983b; Heymsfield and Blackmer 1988; Adler et al. 1985, Brunner et al. 2007). Enhanced longwave InfraRed (IR) satellite imagery of deep convection sometimes displays this cloud-top V-shaped feature, in which an equivalent blackbody temperature (BT) region of a storm is enclosed by a V-shaped region of colder BT (see figure1; Negri 1982; McCann 1983; Heymsfield et al. 1983a, 1983b; Fujita 1982). The enhanced-V develops when a strong updraft penetrates into the lower stratosphere and results in an overshooting thunderstorm top (Fig. 1). This overshooting top interacts with strong upper level winds (Fujita 1978, Wang 2007). One hypothesis is that the flow erodes the updraft summit and carries cloud debris downwind resulting in the colder BTs of the enhanced-V feature (McCann 1983). The coldest BT, which is near the apex of the enhanced-V, is associated with adiabatic expansion due to the ascent of air parcels in the thunderstorm updraft region overshooting the tropopause (Heymsfield and Blackmer 1988; Adler and Mack 1986). Several hypotheses have been proposed to explain the warm region of BTs enclosed by the V-feature. One hypothesis argues that the region is a result of subsidence of negatively buoyant overshooting cloud air downstream of an ascending cloud top (Heymsfield and Blackmer 1988; Adler and Mack 1986; Heymsfield et al. 1983a; Negri 1982; Schlesinger 1984). A second hypothesis has been proposed which explains the warm region on the basis of radiative properties of the cloud particles. Based on radiative transfer simulations and assuming that the ice water content varied spatially across the anvil, Heymsfield et al. (1983b) found that the interior warm region had lower ice water content compared to the V-arms. This situation implies a smaller optical depth in the warm region and warmer BTs

characteristic of lower altitudes. Another hypothesis argues that stratospheric cirrus (Fujita 1982) generated in the wake of overshooting tops is sinking into the anvil. Located above an anvil top and at a warmer environmental temperature, the stratospheric cirrus appears warmer in the BTs sensed by the IR satellite channel (Wang et al. 2002; Setvak et al. 2007). A fourth hypothesis describes gravity waves and lee waves produced by the storms as the cause to the warm region downwind of the coldest BT (Stobie 1975; Heymsfield et al. 1991; Wang 2007).

The presence of enhanced-V features signifies strong tropospheric shear and intense updrafts, both of which are also essential for severe thunderstorms (Heymsfield and Blackmer 1988). The presence of enhanced-Vs is associated with severe weather (McCann 1983; Negri 1982; Heymsfield et al. 1983a, 1983b; Adler et al. 1985; Heymsfield and Blackmer 1988). McCann (1983) explored the association of enhanced-Vs to severe weather reports, suggesting a possible application for severe weather warnings. He found a 30-minute median lead time from the time the enhanced-V appeared in enhanced IR imagery to the time of the first report of severe weather. In addition, he found that most of the enhanced-Vs studied were associated with severe weather (i.e., low False Alarm Ratio (FAR)). However, a large number of severe storms did *not* have an enhanced-V (low Probability Of Detection (POD)).

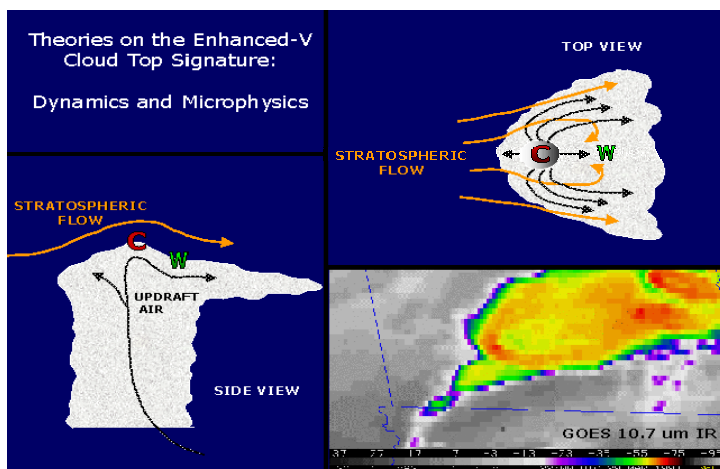


Figure 1: Theories on the Enhanced-V Cloud Top Signature (from Enhanced-V VISIT Training Lesson, Scott Bachmeier, 1999).

2. BASIS FOR DETECTION ALGORITHM

The enhanced-V parameters to use for the temperature couplet detection are described and listed below:

- 1) TMIN: the minimum cloud top equivalent blackbody temperature (BT) observed in the overshooting top region. TMIN is usually near the apex of the enhanced-V and is associated with adiabatic expansion owing to air parcels in the thunderstorm updraft region overshooting the tropopause (Heymsfield and Blackmer 1988; Adler and Mack 1986). The latitude and longitude of TMIN were recorded and used as the reference position of each enhanced-V.
- 2) TMAX: the maximum cloud top BT detected within an embedded warm area downwind of TMIN. Refer to Figure 2a for an example of TMIN and TMAX. For this enhanced-V case, TMIN and TMAX were observed to have values of 192 K (-81° C) and 212 K (-61° C), respectively.
- 3) TDIFF: the difference in cloud top BTs between TMIN and TMAX which forms a cold-warm couplet (McCann 1983; Heymsfield et al. 1983a, 1983b; Negri 1982; Fujita 1982).
- 4) DIST: the distance between TMIN and TMAX. Refer to Figure 2b for an example of TDIFF and DIST. For this case, TDIFF and DIST were observed to have values of 20 K and 7 km, respectively.

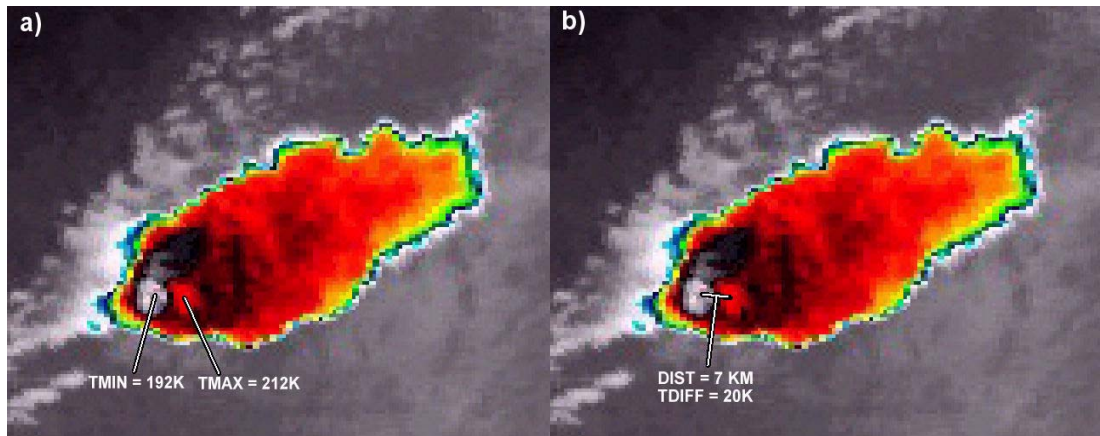


Figure 2: A NOAA-AVHRR 1 km spatial resolution enhanced 10.8 μm IR channel image over southwestern Texas at 2102 UTC on 9 May 2003. The enhanced-V quantitative parameters associated with temperature couplet detection are labeled in the two panels (a) TMIN (K) and TMAX (K) (b) TDIFF (K) and DIST (km).

Two Low Earth Orbit (LEO) satellite datasets that included the 10.7, 10.8, and 11 μm InfraRed (IR) channels were obtained over the continental United States for the enhanced-V study. These satellite datasets provide a 1 km ground sampled distance and consisted of:

- National Oceanic and Atmospheric Administration (NOAA)-Advanced Very High Resolution Radiometer (AVHRR) and National Aeronautics and Space Administration (NASA)-Earth Observing System's (EOS) MODerate-resolution Imaging Spectroradiometer (MODIS) AQUA and TERRA overpasses from 4 May 2003 to 5 July 2003. There were 209 enhanced-V cases collected in the 2003 season.
- NOAA-AVHRR and NASA-EOS MODIS AQUA and TERRA overpasses from 1 May 2004 to 1 July 2004. There were 241 enhanced-V cases collected in the 2004 season.

Refer to Table 1 for results of the quantitative parameters of the enhanced-V feature for both seasons. The mean and median values of the enhanced-V parameters represent the “average” for the enhanced-V features identified by visual inspection. Also, the minimum and maximum values show the extremes of the enhanced-V parameters for the two seasons. These values for the four parameters form the basis of deciding the threshold values to choose in the temperature couplet algorithm. The thresholds were chosen that included at least 50 percent of the cases from the 2003 and 2004 seasons. A brightness temperature difference threshold between the water vapor and longwave infrared channels is used to detect overshooting top pixels. There have been some studies that have utilized this channel difference for overshooting top detection (Schmetz et al. 1997; Setvak et al. 2007). The main principle is that above deep convective clouds, the water vapor band is warmer than the longwave infrared window band (Ackerman 1996).

The enhanced-V parameters TMIN, TMAX, and TDIFF were compared at different ground sampled distances for an enhanced-V case to see if varying ground sampled distance has an effect on these parameters. The enhanced-V feature was observed at 1 km, 2 km, 4 km, and 8 km ground sampled distances and is shown in Figure 3. The TMIN enhanced-V parameter got warmer as the ground sampled distance got coarser (i.e., 4 and 8 km) (Table 2). In fact, TMIN was observed at 11 K warmer for the LEO 8 km ground sampled distance compared to the 1 km ground sampled distance. The warmer TMIN values were observed for the 4 and 8 km ground sampled distances because at these ground sampled distances, the satellite imagery could not resolve the overshooting top regions adequately. However, since the representative diameter of an overshooting top is commonly known to be around 1 or 2 km, satellite imagery observed at 1 or 2 km ground sampled distance could resolve the overshooting top regions adequately (Igau et al. 1999, LeMone and Zipser 1980). The TMAX parameter values got slightly colder for coarser ground sampled distances, but only changed by 4 K from 1 km to 8 km ground sampled distances (Table 2). This seems to be because the temperature region associated with TMAX occurs over a relatively large area (compared to TMIN) and can be resolved fairly well for both finer (1 km) and coarser (8 km) ground sampled distances. The DIFF parameter values decreased significantly (15 K) from finer (1 km) to coarser (8 km) LEO ground

sampled distance (Table 2). These temperature couplet value changes were affected mainly by TMIN since the value of TMAX did not change much from 8 km to 1 km ground sampled distances.

2003 SEASON:		209 CASES		
PARAMETER	MEAN	MEDIAN	MAXIMUM	MINIMUM
TMIN (K)	201	200	222	184
TMAX (K)	217	217	246	205
TDIFF (K)	16	16	35	5
DIST (km)	11	10	43	3
2004 SEASON:		241 CASES		
PARAMETER	MEAN	MEDIAN	MAXIMUM	MINIMUM
TMIN (K)	201	201	220	181
TMAX (K)	217	217	232	206
TDIFF (K)	16	15	41	5
DIST (km)	10	9	41	3

Table 1: The Mean, Median, Maximum, and Minimum values for TMIN (K), TMAX (K), TDIFF (K), and DIST (KM) for the 2003 and 2004 enhanced-V seasons.

Enhanced-V Parameter	1 km Ground Sampled Distance	2 km Ground Sampled Distance	4 km Ground Sampled Distance	8 km Ground Sampled Distance
TMIN	186 K (-87° C)	188 K (-85° C)	193 K (-80° C)	197 K (-76° C)
TMAX	219 K (-54° C)	218 K (-55° C)	216 K (-57° C)	215 K (-58° C)
TDIFF	33 K	30 K	23 K	18 K

Table 2: BT values for the enhanced-V parameters TMIN, TMAX, and TDIFF for an enhanced-V feature observed from LEO satellite imagery at 1 km, 2 km, 4 km, and 8 km ground sampled distance over northeast Oklahoma at 2218 UTC on 6 May 2003.

3. METHODOLOGY OF DETECTION ALGORITHM

The overshooting top/temperature couplet part of the algorithm consists of a series of threshold tests. The threshold tests for MODIS and GOES cases are described below. If all of the tests are met, then a temperature couplet is detected. The thresholds to detect overshooting tops/temperature couplets are less strict for the GOES cases because of the coarser spatial resolution of the data.

STEP 1: Identify overshooting top pixels

For MODIS cases, pixels assigned as overshooting tops if $[BT(6.7)-BT(11) \geq 6K]$
 For GOES cases, pixels assigned as overshooting tops if $[BT(6.5)-BT(10.7) \geq 0K]$

STEP 2: Identify temperature couplets

For MODIS cases, for each identified overshooting top pixel; $[BT(11) \leq 205K]$, $[BT(11) \text{ Difference between cold and warm pixel} \geq 15K \text{ and} \leq 35K]$, $[BT(6.7)-BT(11) \geq 0K \text{ of warm pixel}]$, and $[Distance \text{ between cold and warm pixel} \leq 20 \text{ km}]$.

For GOES cases, for each identified overshooting top pixel; $[BT(10.7) \leq 215K]$, $[BT(10.7) \text{ Difference between cold and warm pixel} \geq 6K \text{ and} \leq 25K]$, $[BT(6.5)-BT(10.7) \geq -2K \text{ of warm pixel}]$, and $[Distance \text{ between cold and warm pixel} \leq 20 \text{ km}]$

The threshold for the brightness temperature difference between the water vapor and longwave infrared channels for the warm pixel was used to eliminate clear sky pixels falsely identified as warm pixels. An upper limit threshold was set for the longwave infrared brightness temperature difference between the cold and warm pixels to also prevent clear sky pixels from being falsely identified as warm pixels. The distance threshold was set to limit the search range of the warm pixel from the cold pixel to additionally prevent clear sky pixels and warm pixels further downwind in anvil region as being falsely identified as warm pixels.

Additionally, the warm pixel location is restricted to be downwind, in the eastern 180-degree quadrant compared to the cold pixel location. Also, the warm pixel temperature is averaged for a 3x3 box

surrounding the pixel to further eliminate erroneous single false warm pixels. The magnitude and angle orientation of the detected temperature couplet is also calculated.

STEP 3: Identify enhanced-V features

Orient the enhanced-V fabricated matrix in the direction of the temperature couplet angle orientation. Search for the enhanced-V features around the temperature couplet regions (specifically a 50x50 pixel box around the overshooting top pixel location associated with the temperature couplet). The enhanced-V cross correlation algorithm will search in the region of temperature couplets for correlations between the enhanced-V and the enhanced-V fabricated matrix.

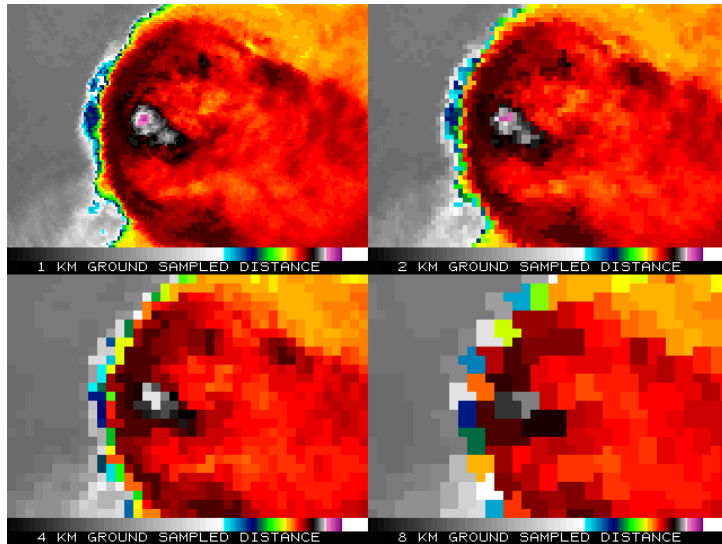


Figure 3: Enhanced-V feature located over northeast Oklahoma observed from LEO satellite imagery at 2218 UTC on 6 May 2003 for 1 km, 2 km, 4 km, and 8 km ground sampled distances. The purple and white colors in the location of the updraft and overshooting top represent colder BTs, while the surrounding black and red colors represent warmer BTs.

4. CASE STUDIES

The following two cases illustrate how the algorithm performs with satellites of different resolution. The main problem is to minimize false detection of temperature couplets without missing true temperature couplets. The results presented highlight this problem and an additional threshold check will be implemented into the algorithm to attempt to alleviate the problem. This check will remove any consideration of a temperature couplet if a pixel aligned along the temperature couplet orientation at a distance of 20 km beyond the prospective warm pixel has a $BT(6.7) - BT(11) < 0K$ for MODIS and $BT(6.5) - BT(10.7) < -2K$ for GOES. The goal with this additional check is to eliminate the false detection of temperature couplets along the anvil edge.

CASE 1:

The first case study was from 7 April 2006 at 1710 UTC over Tennessee. Figure 4 shows the temperature couplets identified on the MODIS (left) and GOES (right) images. There were four main storms observed on the satellite imagery. The MODIS temperature couplet algorithm was successful in identifying temperature couplets along with the correct orientation of the couplets toward the northeast in storms 1 and 2. Also, a temperature couplet was detected in storm 4 but it did not have the correct angle orientation. Further, false detections of temperature couplets along the anvil edge occurred in storm 4. In addition, a false detection of a temperature couplet along the anvil edge occurred in storm 3. The GOES temperature couplet algorithm successfully identified temperature couplets in storms 2 and 4. The angle orientation of the temperature couplet was correctly identified in storm 2 toward the northeast, but was not identified correctly in storm 4. Also, false detections of temperature couplets along the anvil edge occurred in storm 4. No temperature couplets were identified in storms 1 and 3 for the GOES data.

CASE 2:

The second case study was from 25 May 2004 at 0430 UTC for MODIS case and at 0432 UTC for GOES case over Oklahoma and Illinois. Figure 5 shows the temperature couplets observed on the MODIS (left) and GOES (right) images for a storm over Oklahoma. The MODIS temperature couplet algorithm successfully identified a temperature couplet with an angle orientation of the couplet toward the northeast. However, there were false detections of temperature couplets along the anvil edge as well. The GOES temperature couplet algorithm identified false detections of temperature couplets along the anvil edge but no true couplet. Figure 6 shows the temperature couplets observed on the MODIS (left) and GOES (right) images for storms over Illinois. The MODIS temperature couplet algorithm successfully identified temperature couplets with a correct angle orientation toward the southeast. There were no false detections of temperature couplets identified. The GOES temperature couplet algorithm identified temperature couplets successfully with a correct angle orientation toward the southeast but also identified numerous false detections of temperature couplets along the anvil edge.

5. FUTURE WORK

There are three main additional steps to focus on for this project. The first step is to revise the overshooting top/temperature couplet algorithm to minimize false detection of temperature couplets and to detect more temperature couplets. The second step is to develop the enhanced-V cross-correlation algorithm by searching in the region of temperature couplets for correlations between the enhanced-V and the enhanced-V fabricated matrix. The third step is to test the overshooting top/temperature couplet/enhanced-V algorithm on several years of cases. With these improvements and extensions, the algorithm should prove useful for operations with future sensors, such as the Advanced Baseline Imager (ABI) on GOES-R (Schmit et al. 2005).

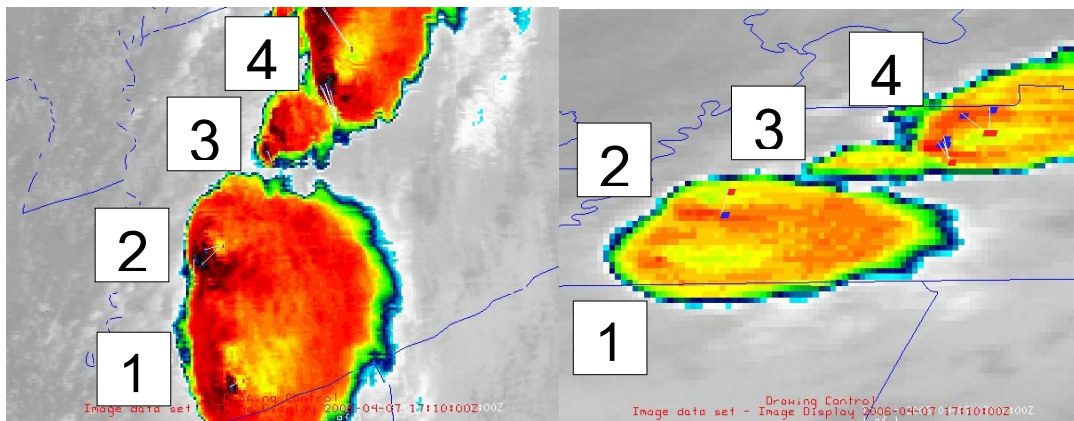


Figure 4: MODIS enhanced 11-micron image with temperature couplet algorithm results for case over Tennessee on 7 April 2006 at 1710 UTC (left) and GOES enhanced 10.7-micron image with temperature couplet algorithm results at same time (right). White lines denote temperature couplets, blue box denotes cold pixel, and red box denotes warm pixel.

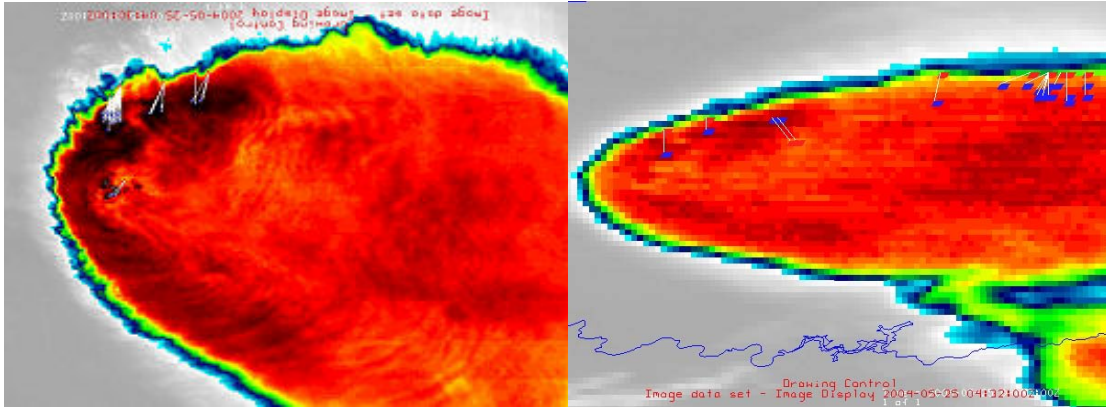


Figure 5: MODIS enhanced 11-micron image with temperature couplet algorithm results for case over Oklahoma on 25 May 2004 at 0430 UTC (left) and GOES enhanced 10.7-micron image with temperature couplet algorithm results for same case on 25 May 2004 at 0432 UTC (right). White lines denote temperature couplets, blue box denotes cold pixel, and red box denotes warm pixel.

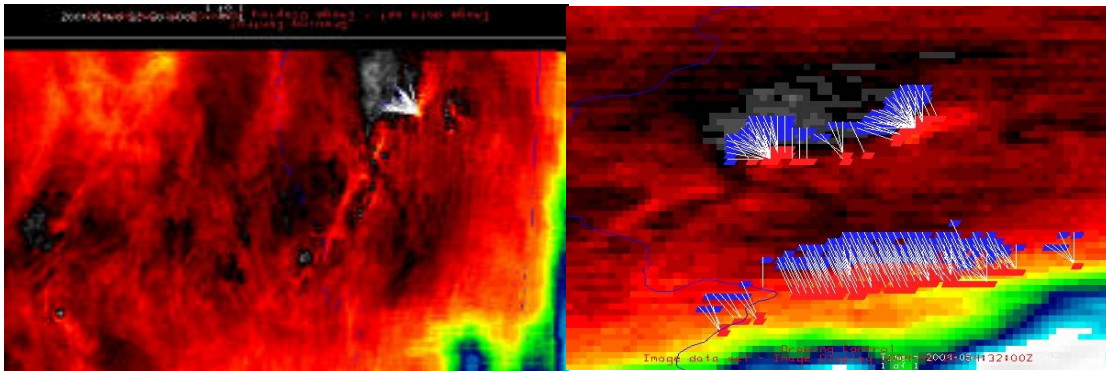


Figure 6: MODIS enhanced 11-micron image with temperature couplet algorithm results for case over Illinois on 25 May 2004 at 0430 UTC (left) and GOES enhanced 10.7-micron image with temperature couplet algorithm results for same case on 25 May 2004 at 0432 UTC (right). White lines denote temperature couplets, blue box denotes cold pixel, and red box denotes warm pixel.

6. ACKNOWLEDGMENTS

The authors would like to thank NASA for allowing us the opportunity to develop the algorithms under grant NNX07AF75G. Also, special thanks to Kris Bedka (SSEC/CIMSS, University of Wisconsin-Madison), Scott Bachmeier (SSEC/CIMSS, University of Wisconsin-Madison), and Tim Schmit (NOAA/NESDIS, Satellite Applications and Research, Advanced Satellite Products Branch, University of Wisconsin-Madison) for providing suggestions and input into the development of the algorithms.

7. REFERENCES

- Ackerman, S. A., 1996: Global satellite observations of negative brightness temperature differences between 11 and 6.7 micron. *Journal of Atmospheric Science*, **53**, 2803-2812.
- Adler, R. F., and R. A. Mack, 1986: Thunderstorm cloud top dynamics as inferred from satellite observations and a cloud top parcel model. *Journal of Atmospheric Science*, **43**, 1945-1960.
- Adler, R. F., M. J. Markus, and D. D. Fenn, 1985: Detection of severe Midwest thunderstorms using geosynchronous satellite data. *Monthly Weather Review*, **113**, 769-781.
- Brunner, J. C., S. A. Ackerman, A. S. Bachmeier, and R. M. Rabin, 2007: A Quantitative Analysis of the Enhanced-V Feature in Relation to Severe Weather. *Wea. Forecasting*, **22**, 853-872.
- Fujita, T. T., 1978: Manual of downburst identification for Project NIM-ROD. SMRP 156, University of Chicago, 104 pp.

Fujita, T. T., 1982: Principle of stereoscopic height computations and their applications to stratospheric cirrus over severe thunderstorms. *Journal of Meteorological Society of Japan*, **60**, 355-368.

Heymtsfield, G. M., and R. H. Blackmer, Jr., 1988: Satellite-observed characteristics of Midwest severe thunderstorm anvils. *Monthly Weather Review*, **116**, 2200-2224.

Heymtsfield, G. M., R. H. Blackmer, Jr., and S. Schotz, 1983: Upper level structure of Oklahoma tornadic storms on 2 May 1979, Pt. 1 radar and satellite observations. *Journal of Atmospheric Science*, **40**, 1740-1755.

Heymtsfield, G. M., R. Fulton, and J. D. Spinhirne, 1991: Aircraft overflight measurements of Midwest severe storms: Implications on geosynchronous satellite interpretations. *Monthly Weather Review*, **119**, 436-456.

Heymtsfield, G. M., G. Szejwach, S. Schotz, and R. H. Blackmer, Jr., 1983: Upper level structure of Oklahoma tornadic storms on 2 May 1979, Pt. 2 Proposed explanation of "V" pattern and internal warm region in infrared observations. *Journal of Atmospheric Science*, **40**, 1756-1767.

Igau, R.C., M.A. LeMone, and D. Wei, 1999: Updraft and Downdraft Cores in TOGA COARE: Why So Many Buoyant Downdraft Cores? *J. Atmos. Sci.*, **56**, 2232-2245.

LeMone, M.A., and E.J. Zipser, 1980: Cumulonimbus Vertical Velocity Events in GATE. Part I: Diameter, Intensity and Mass Flux. *J. Atmos. Sci.*, **37**, 2444-2457.

McCann, D. W., 1983: The enhanced-V: A satellite observable severe storm signature. *Monthly Weather Review*, **111**, 887-894.

Negri, A. J., 1982: Cloud-top structure of tornadic storms on 10 April 1979 from rapid scan and stereo satellite observations. *Bulletin of the American Meteorological Society*, **63**, 1151-1159.

Schlesinger, R. E., 1984: Mature thunderstorm cloud-top structure and dynamics: A three-dimensional numerical simulation study. *Journal of Atmospheric Science*, **41**, 1551-1570.

Schmetz, J., Tjemkes, S. A., Gube, M., van de Berg, L., 1997: Monitoring deep convection and convective overshooting with METEOSAT. *Adv. Space Res.*, **19**, 433-441.

Schmit, T. J., M. M. Gunshor, W. P. Menzel, J. J. Gurka, J. Li, and A. S. Bachmeier, 2005: Introducing the Next-generation Advanced Baseline Imager (ABI) on Geostationary Operational Environmental Satellites (GOES)-R. *Bulletin of the American Meteorological Society*, **8**, 1079-1096.

Setvak, M., R. M. Rabin, and P. K. Wang, 2007: Contribution of the MODIS instrument to observations of deep convective storms and stratospheric moisture detection in GOES and MSG imagery. *Atmospheric Research*, **83**, 505-518.

Stobie, J. G., 1975: Gravity shear waves atop the cirrus layer of intense convective storms. NASA Contractor Report, NASA-CR-147140, Colorado State University, 128 pp.

Wang, P. K., 2007: The Thermodynamic Structure atop a Penetrating Convective Thunderstorm. *Atmospheric Research*, **83**, 254-262.

Wang, P. K., H-m. Lin, S. Natali, S. Bachmeier, and R. Rabin, 2002: Cloud model interpretation of the mechanisms responsible for the satellite-observed enhanced V and other features atop some Midwest severe thunderstorms. *Proceedings of the 11th American Meteorological Society Conference on Cloud Physics*, Ogden, UT, June 3-7, 2002.